THE ARCHIVE OF MECHANICAL ENGINEERING

Vol. XLIX 2002 Number 3

Key words: *aerodynamics, ornithopter, flapping wings*

JAN WOJCIECHOWSKI[*)]

EXPERIMENTAL INVESTIGATION OF AERODYNAMIC FORCES GENERATED ON ORNITHOPTER MODEL IN WIND TUNNEL

The measurement of lift and drag forces on the ornithopter model with flapping wings was carried out in the wind tunnel. The wing movement had two degrees of freedom: flapping (around the longitudinal axis of the model) and feathering (around the wing axis). Forces were measured in static case – as averaged values during many cycles of movement, and in dynamic case – as unsteady forces captured in function of the flapping phase. The magnitudes of the aerodynamic coefficients of lift and drag were calculated.

1. Phenomenological description

Within 13.000 species of warm-blooded animals existing now, 10.000 species have developed flying as the mode of moving (9000 species of birds and 1000 species of bats, passing over the single species of flying squirrels, lizards or fish) – see Dial [1]. Moreover, nearly one million species of insect flies.

The comparison of the velocity of displacement, expressed in body length per second and based on the average velocity at maximal power output for the individuals from different species, repeated after W. Shyy [2], is reported in Tab. 1.

Table 1.

Species	Velocity body length / sec
man	3–4
race horse	7
cheetah	18
SR71 Blackbird at M=3	32
goose	50

*) *Institute of Aeronautics and Applied Mechanics, Warsaw University of Technology; ul. Nowowiejska 24, 00-665 Warszawa, Poland; E-mail: jan@meil.pw.edu.pl*

pigeon	75
starling	120
swallow	140
midge	250
honeybee	300
house fly	400

Using the set of flying species and engineering constructions reported by H.Tennekees [3] in the range from midge to Boeing, with some broadening of the analysis presented by W.Shee [2], one can obtain some correlation scaling the mechanism of wing work in stationary flight for the group of birds:

- Lift force P[N] (and body weight) is related to the flight velocity v [m/s] as $P = 10^{-6} v^6$,
- Wing span B[m] for birds within the range of P from 0.1 to 10 N, is correlated by: $B = 0.5 \cdot P^{1/3}$,
- Wing area S [m^2] is given by: $S = 0.03 \cdot P^{0.72}$
- Wing flapping frequency F [Hz]: $F = 7 \cdot P^{-0.28}$

On the basis of those data, for the ornithopter with the weight 1 N one can found the flight velocity v = 10m/s, using the wings with span B=0.5 m and area S=0.03m^2, flapping at F = 7Hz.

The main goal of the reported work was to estimate of the aerodynamic forces generated in the ornithopter model of such scale, mounted on a balance in the wind tunnel. The main application of the obtained results was the furniture of reference data for the numerical computing, realized in parallel.

2. The model, its design and kinematics.

The ornithopter model was equipped with two rigid wings. Their parameters are shown in Tab. 2.

Table 2.

profile	length b[m]	chord c[m]	rel. thick. [-]	dist. axis-end[m]	mass [g]
Clark Y	0.2	0.08	0.12	0.24	25

The measurements were carried out at the wing flapping frequency f = 5 Hz. The velocities, Reynolds and Strouhal numbers used during the experiments are specified in Tab. 3.

Table 3.

Nr	velocity V m/s	Re = V c / ν	St = c f / V
1	0	0	–
2	8	42 000	0.05
3	12	65 000	0.033
4	14	75 000	0.029
5	16	85 000	0.025

The mechanism of the ornithopter is shown schematically in Fig. 1. It allows two degrees of freedom of wing movement:

a) flapping of the wing around the longitudinal axis of model,
b) feathering around the axis of wing

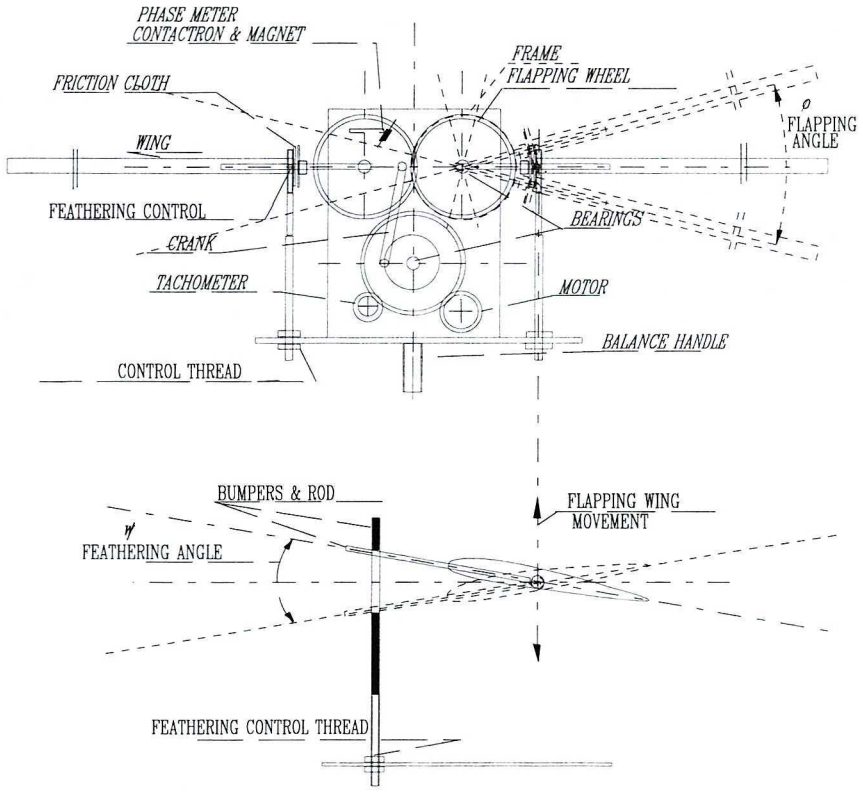

Fig. 1. Scheme of moving wing mechanism (front view) and angle of attack control

The flapping movement is carried out through the crank connecting the drive wheel with one of two gear wheels, in mesh with the other symmetrical. Those wheel's shafts execute the flapping movement of wings. The amplitude of this movement depends on the choice of fixation point of the crank on the drive wheel; while the neutral position is fixed by the crank length. The drive wheel is propelled by an electric motor 24V, 30W. During measurements, the wheel velocity is controlled by the tachometric generator, allowing continuous manual control of the flapping frequency.

In the experiments, the total flapping angle was admitted $\varphi = 40^0$ around the base position 0^0. The flapping frequency was fixed as 5 Hz, 300 rpm.

The feathering angle control is carried out by the wing rotation around its longitudinal axis. The salient rod, perpendicular to the wing axis, is installed on the wing. During flapping movement, this rod moves inside of a bumper window fixed to the chassis. Streaking the window edge, the rod forces the wing to rotate against the resistance of friction cloth. The amplitude of feathering movement $\Delta\psi$, controlled by the opening of the window, was taken equal to $\Delta\psi=20^0$ and $\Delta\psi=10^0$ in two series of experiment. The mean value of the feathering angle ψ was fixed by the vertical displacement of the window and was taken in most part of experiments as $\psi = (+10^0, +5^0, 0^0, -5^0, -10^0)$.

The phase of flapping movement φ was controlled by the contactron installed on the chassis and magnet fixed on the gear wheel. The initial reference point of all the graphs was fixed by the contactron signal, starting at the position 15^0 before the lower dead point of flapping.

The kinematics of the two movements, flapping angle φ and feathering angle ψ, is shown in Fig. 2 in function of the phase angle (angle β of rotation of drive wheel).

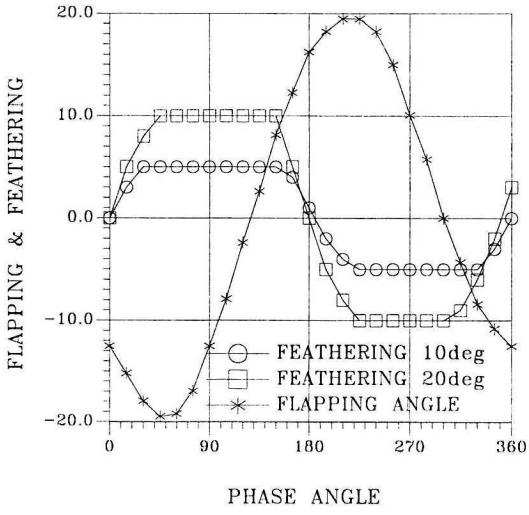

Fig. 2. Wing movement

The vertical movement of the wing end, with velocity V_p relative to the flow velocity V, generates the kinematic angle of attack α_{kin} equal to:

α_{kin} = arc tg (V_p / V) – kinematic angle of attack,

where $V_p = b_c\, \partial\phi/\partial\beta\, f_o$ – velocity of the wing end,

φ – flapping angle,

f_0 – flapping frequency,

V – flight velocity (Tab. 3).

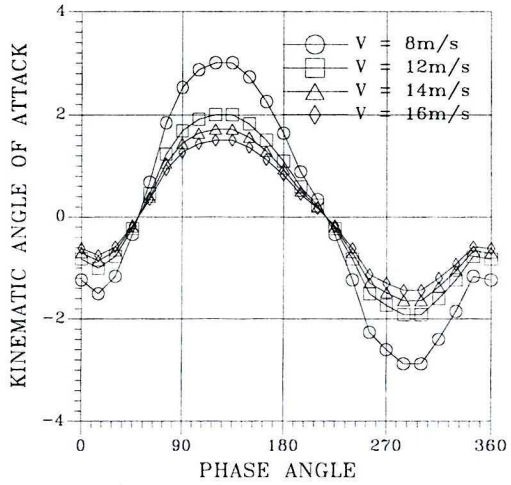

Fig. 3. Kinematic angle of attack

The mean value of α_{kin}, computed for the middle of the wing, is twice lower. The real angle of attack is the trigonometric sum of α_{kin} and feathering angle ψ and is shown for some exemplary (extreme) cases in Fig. 4. The critical angles of attack for Clark Y profile, 15^0 and -12^0, will be overpassed during the movement.

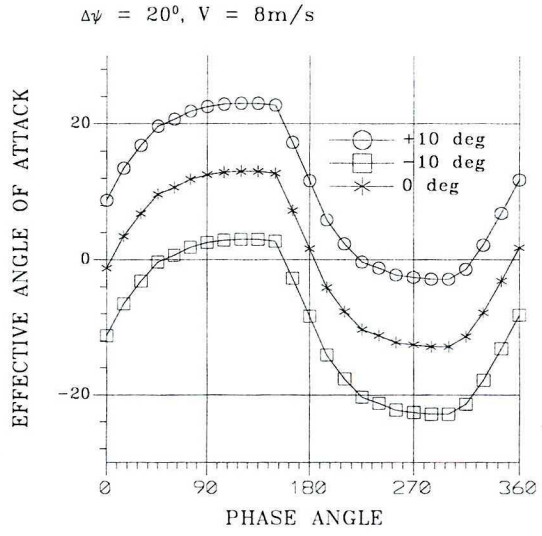

Fig. 4. Real angle of attack – extreme values

3. Results of measurement

The total aerodynamic forces Z and X in the model were measured in two configurations

1. Static measurements – in steady conditions, average forces during flapping movement,
2. Dynamic measurements – unsteady forces in function of phase position of wings.

The measured forces are the effect of four types of efforts:

1. Forces on the model and balance corps (wings dismounted) (Z_k, X_k).
2. Inertial forces, resulting from wing movement in still air (Z_b, X_b).
3. Aerodynamic forces on moving wings (Z_a, X_a).
4. Induced aerodynamic forces between wing and corps of the model (Z_i, X_i).

In the static case, the total forces Z and X were measured, and separately the forces on the model (Z_k, X_k) without wings. Their difference gives the net aerodynamic force (Z_a, X_a).

$$Z_a = Z - Z_k$$
$$X_a = X - X_{jk}$$

In the dynamic case, additionally the inertial forces were enregistrered and then, accordingly in phase, subtracted from total forces. Induction forces were not taken into account.

3.1. Static measurements

The experiments were carried out following the normal procedure in the angle of attack limits from -15^0 to $+20^0$ with step $½^0$. Time of averaging for each point was nearly 3.5 sec., i.e. about 17 flappings. The results are shown in Fig. 5.

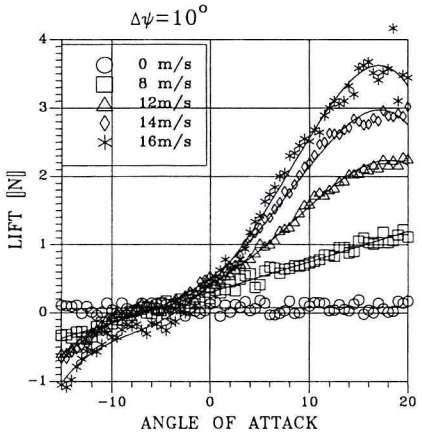

a)

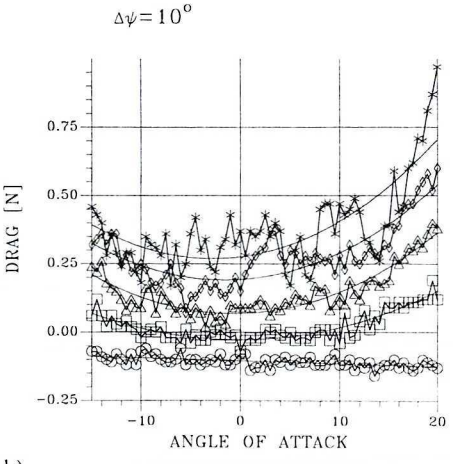

b)

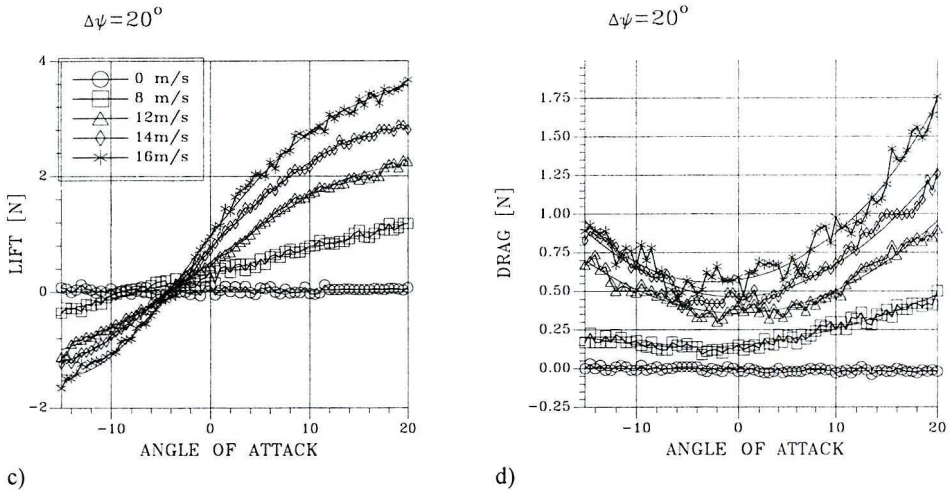

Fig. 5. Lift and drag forces in static measurement for flapping wing:
a) Lift force for $\Delta\psi = 10^0$
b) Drag force for $\Delta\psi = 10^0$
c) Lift force for $\Delta\psi = 20^0$
d) Drag force for $\Delta\psi = 20^0$

The obtained points are shown in the graphs together with the polynomial approximation lines. The visible dispersion of the successive points results from the fact that the forces, for the low velocities of air flow, are extremely weak – of the order of 1N comparing with 100N balance range. For non-zero velocities, the coefficients Cz, Cx were calculated and plotted in Fig. 6. The negative values of Cx indicate positive thrust due to the wing flapping, in the range 0 – 8 m/s for weak amplitude of flapping $\Delta\psi = 10^0$. The dispersion between the Cz and Cx values may manifest the strong dependency on Reynolds number in the Re range of 4 to $8 \cdot 10^4$ (see Tab. 3).

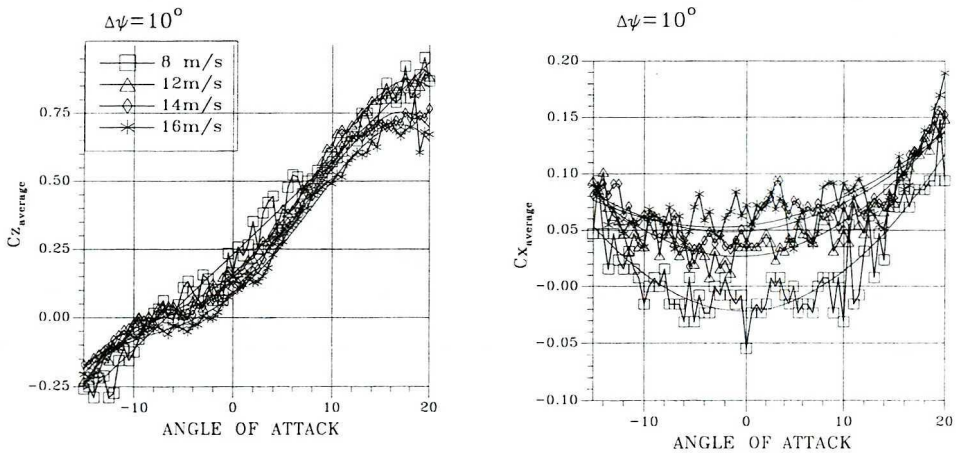

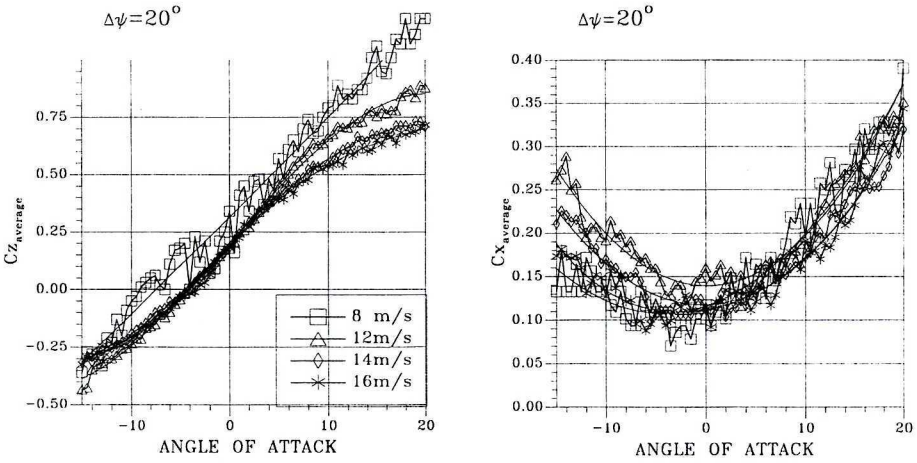

Fig. 6. Lift and drag coefficients in static measurements

3.2. Dynamic measurements

In this case, the model was installed on a 5-composent strain gauge balance, where the electronic system allowed only one component at time. The Z and X components were measured and then the inertia forces Z_b, X_b, measured separately, were subtracted.

Calibration of the system, verified frequently, gave stable coefficients $X_{cal} = 0.42$ [V/N], $Z_{cal} = 0.06$ [V/N] (at the electronic amplification 10). The voltage signal was enregistered with a 12 bit A/C converter in the time of nearly 10 sec (50 flapps) after analogue filtering at 10Hz (drag) and 16 Hz (lift). The proper frequency of the balance vibration with the model was estimated on 45 Hz.

The precision of the measurements, in the sense of obtained time series of forces, may be considered as satisfactory; the time series were repetitive and the phase averaging procedure given the weak differences between the successive cycles. However, the comparison of the average values measured in distinct moments of time showed significant differences. Their source may be related to the properties of balance used in measurements, and particularly to the drift of zero, caused by the corrosion of the contacts in the controlling potentiometers of electronic system of the balance. In addition, during experiments we observed notable level of temperature dependence. We have made an effort to limit those errors in the measure of technical possibilities.

The frequency of flapping was controlled by one side through the tachometer, by other side by following the frequency of the contactron signal on the oscilloscope. It was verified by the spectrum of the signal in some points.

The figures 7 to 10 show the unsteady aerodynamic forces in function of phase angle:

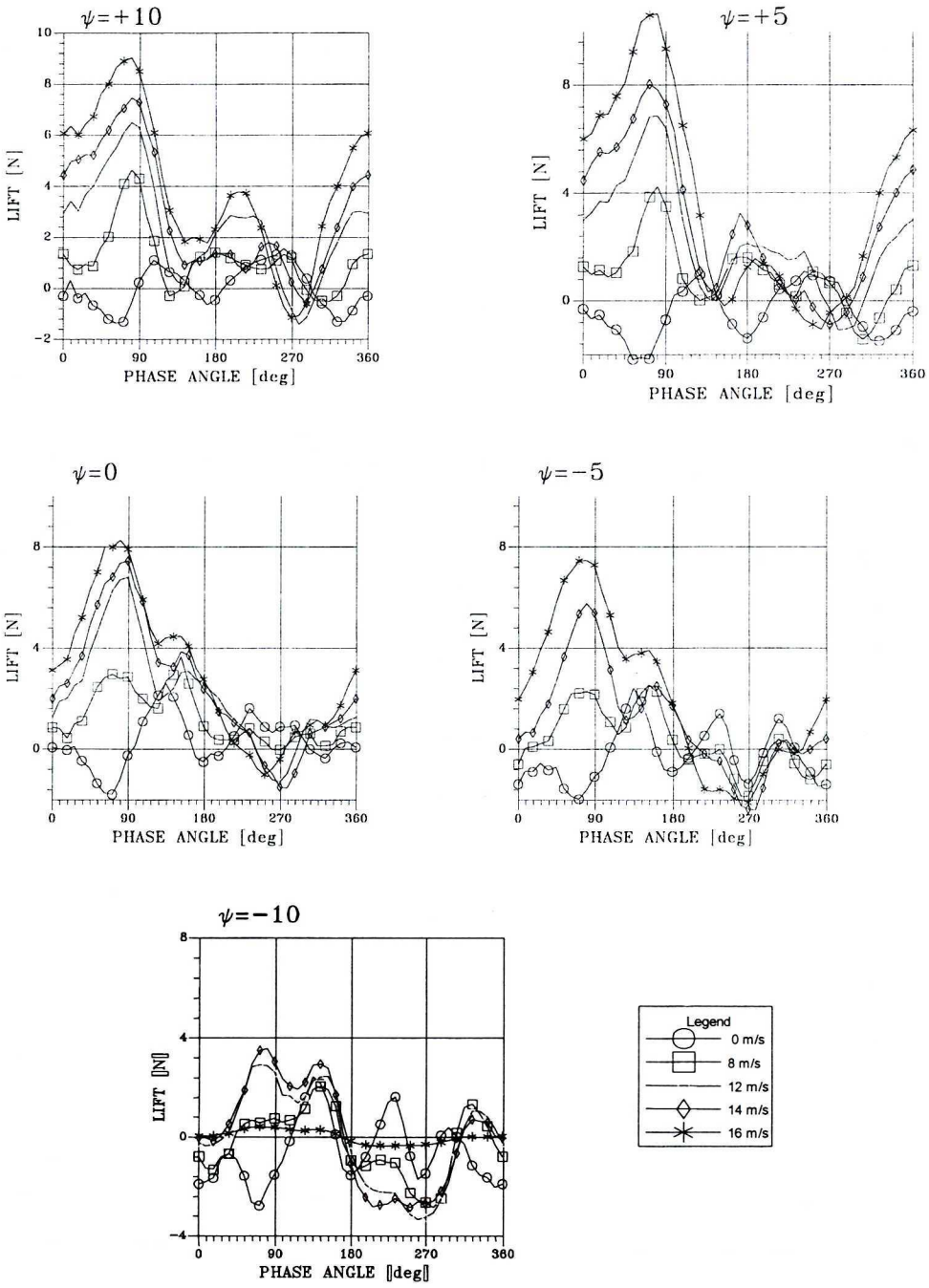

Fig. 7. Unsteady lift force on flapping wing for $\Delta\psi = 20^0$

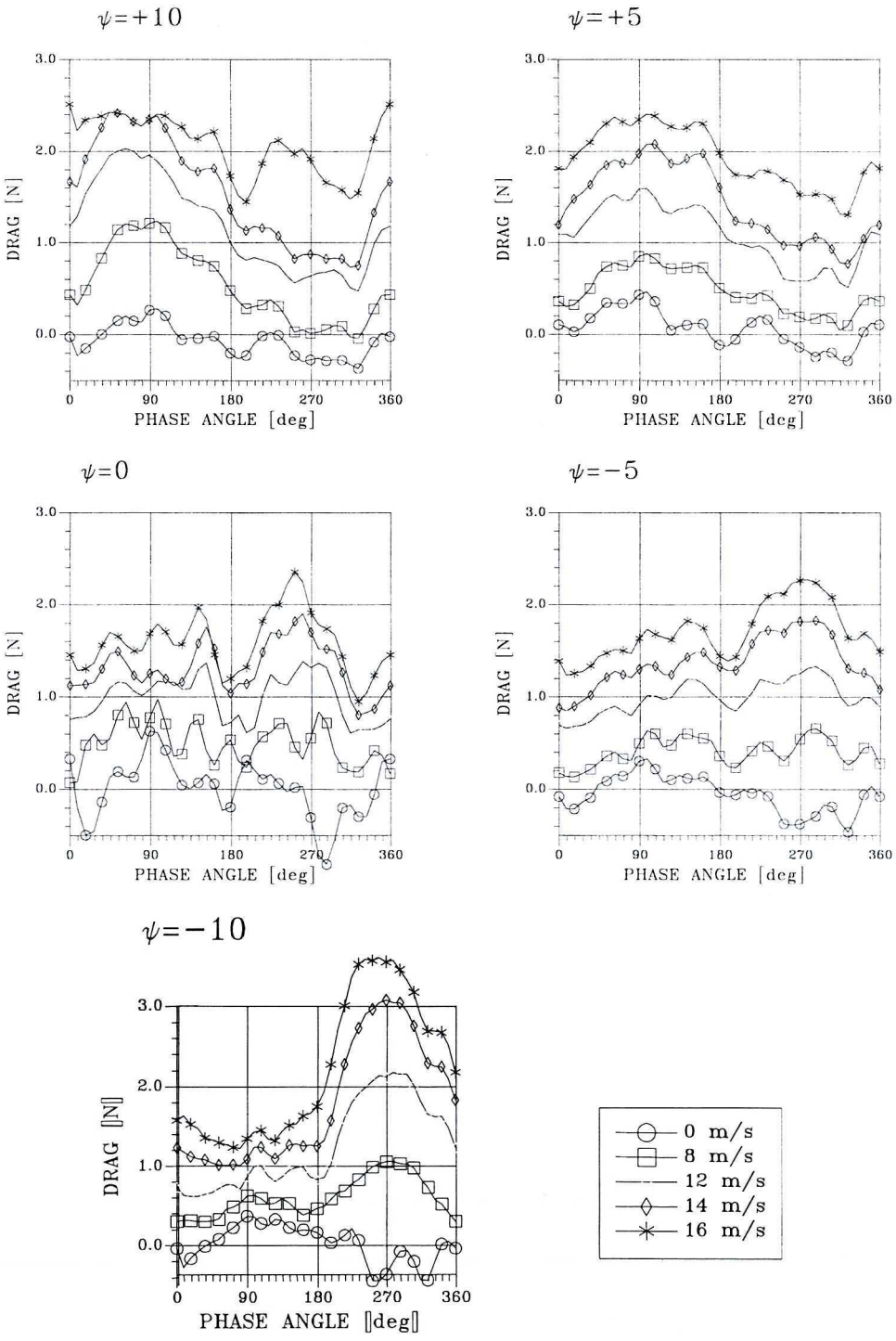

Fig. 8. Unsteady drag force on flapping wing for $\Delta\psi = 20^0$

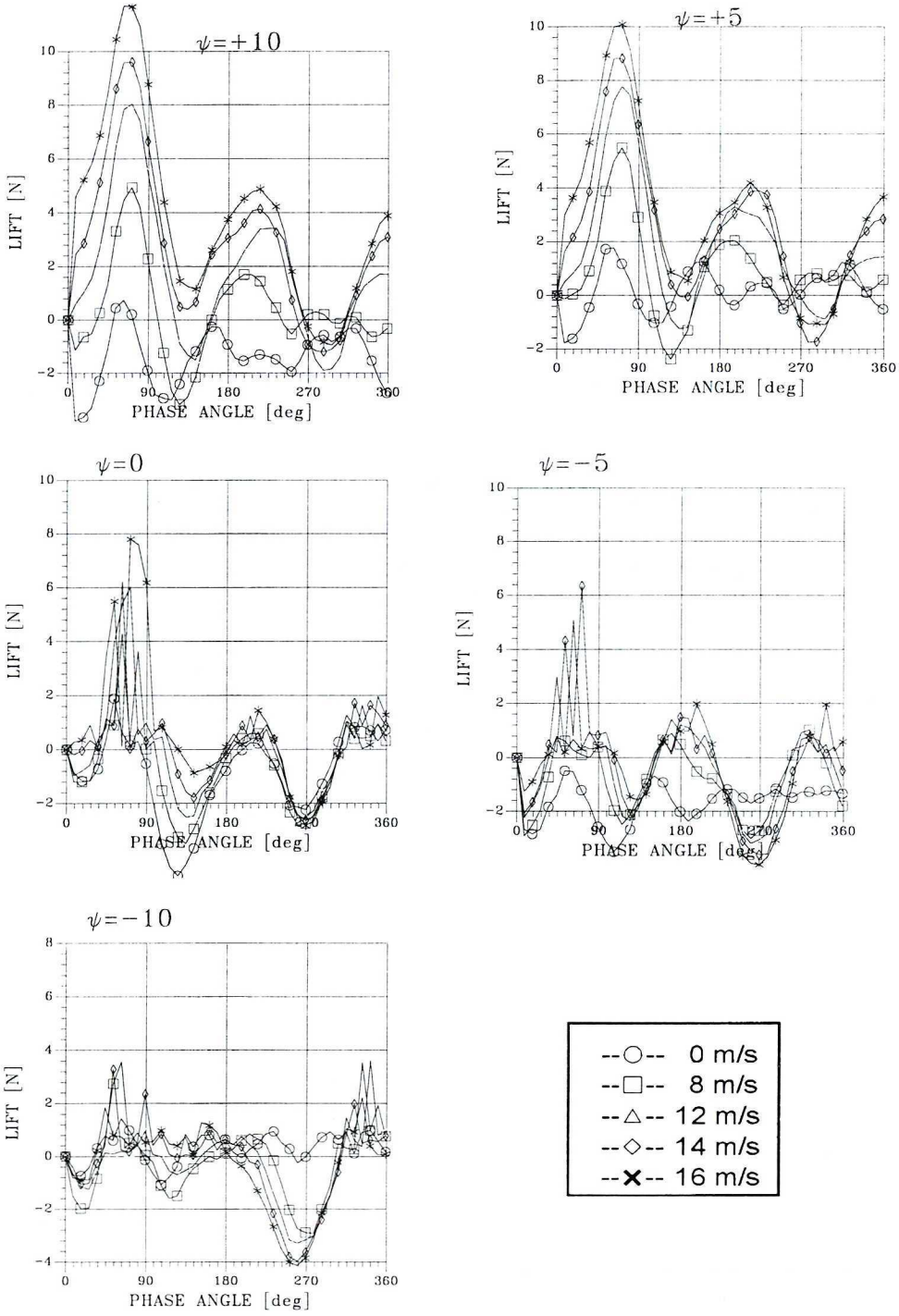

Fig. 9. Unsteady lift force on flapping wing for $\Delta\psi=10^0$

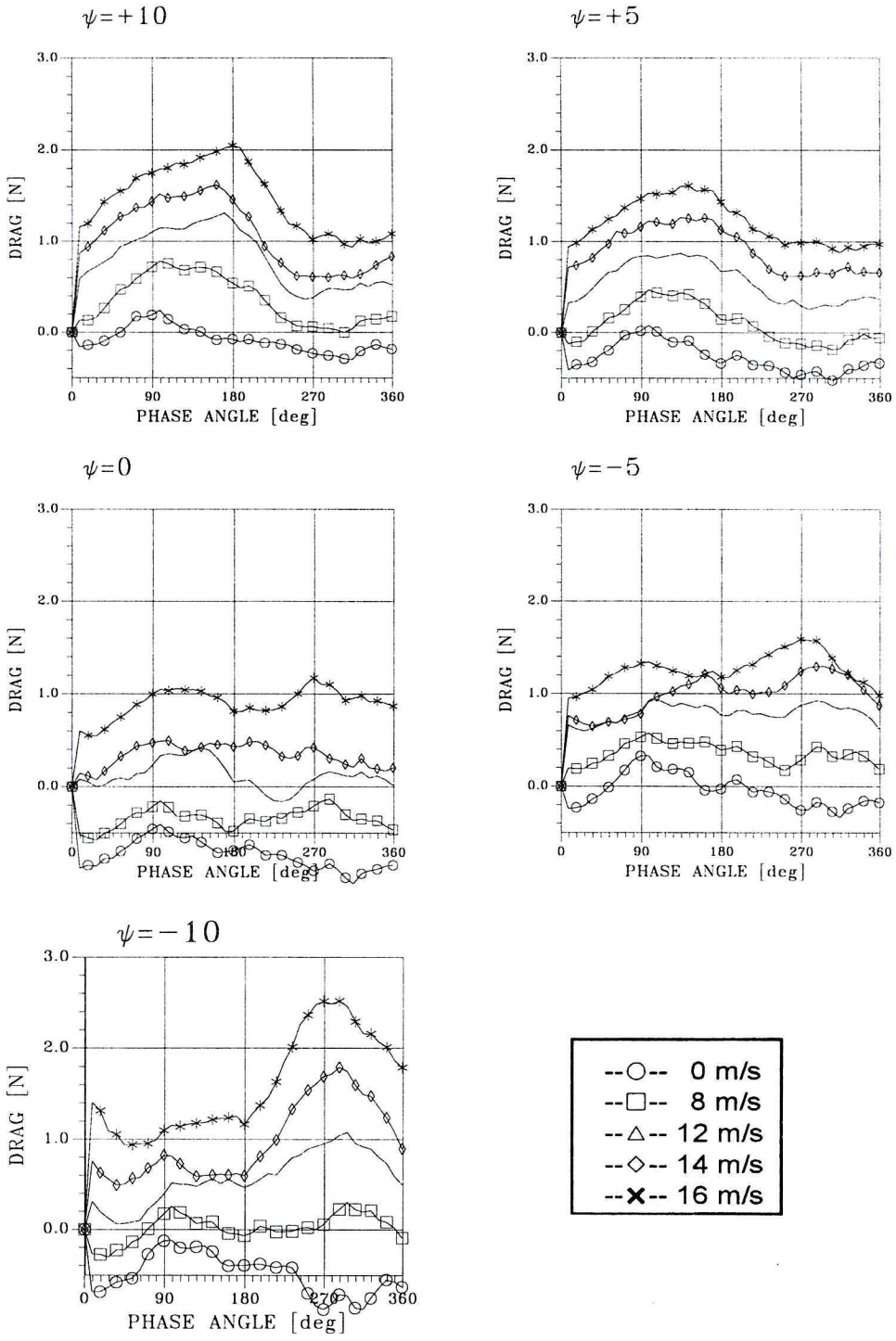

Fig. 10. Unsteady drag force on flapping wing for $\Delta\psi=10^0$

The following values are specified in the Table 4: the lift and drag forces measured for the model corps without wings and the common factor qS depending on velocity V. After subtracting those values from the forces shown in Fig. 7 to 10 and neglecting the results for zero velocity, one obtains the set of Cz and Cz magnitudes as function of phase angle during flapping. The results are presented in Fig. 11 to 14.

Table 4.

V m/s	qS [N]	X0 [N]	Z0 [N]
8	1.28	0.423	1.883
12	2.88	0.807	1.95
14	3.94	1.03	2.20
16	5.12	1.355	2.43

where $q = \rho V^2/2$, $S = 2 \cdot b \cdot c = 0.032\ m^2$

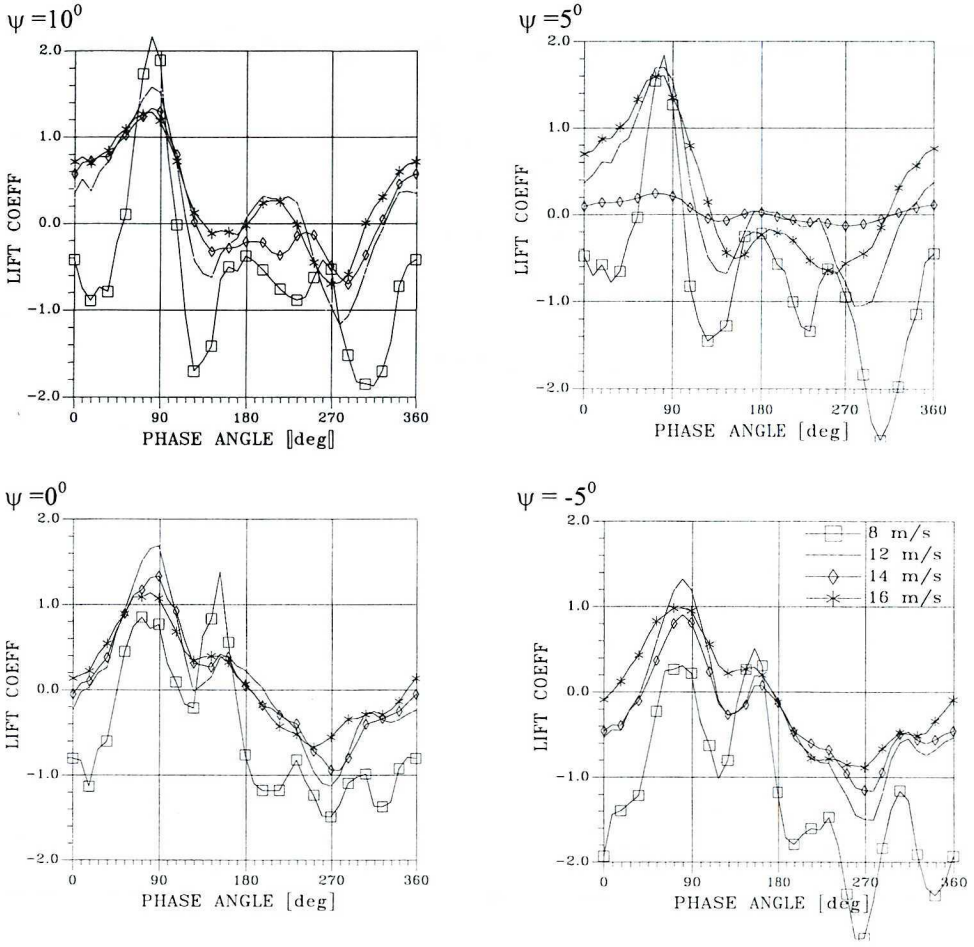

Fig. 11. Unsteady lift coefficient in function of phase angle for $\Delta\psi = 20^0$, $\psi = +10^0$ to -5^0

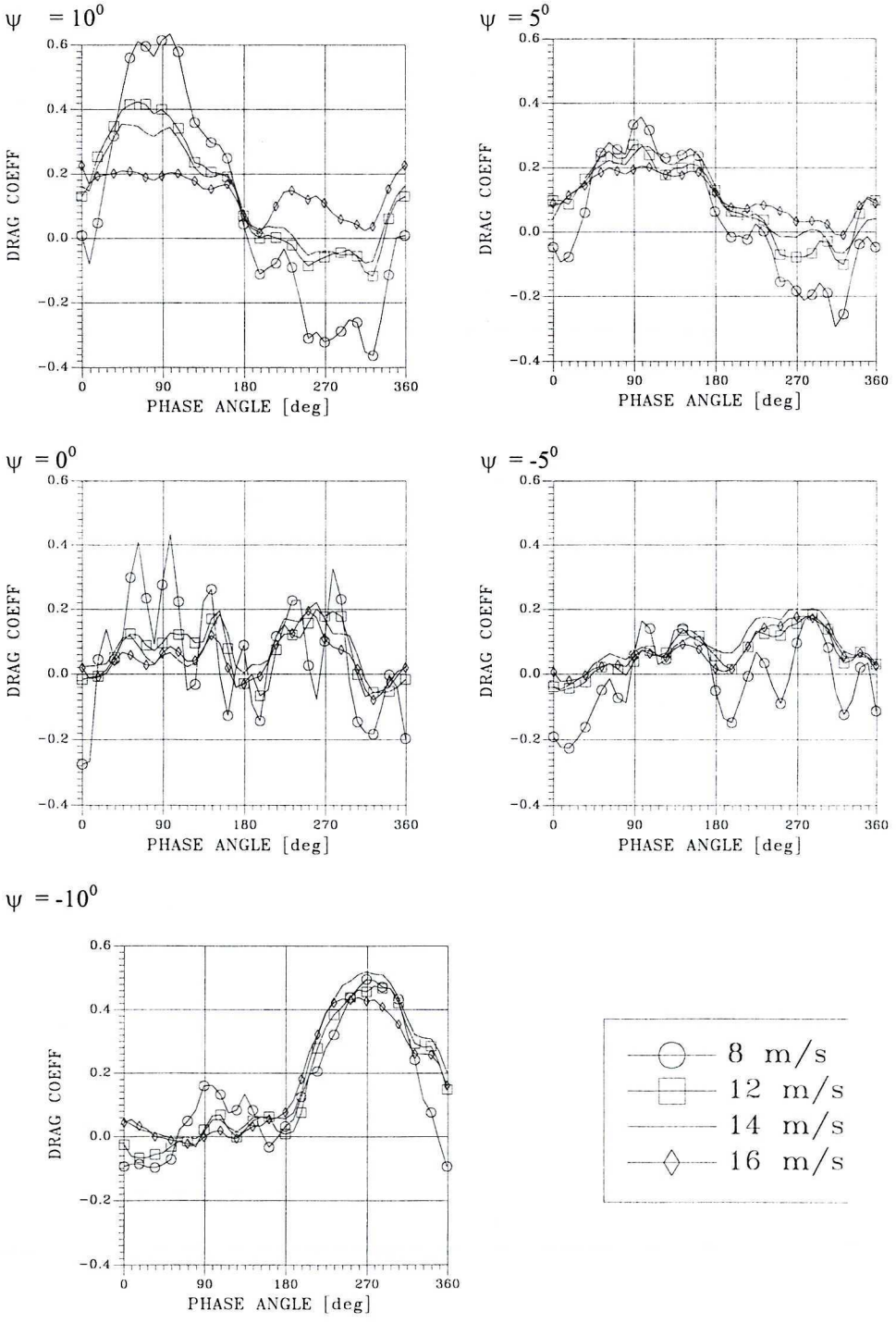

Fig. 12. Unsteady drag coefficient in function of phase angle for $\Delta\psi = 20^0$, $\psi = +10^0$ to -10^0

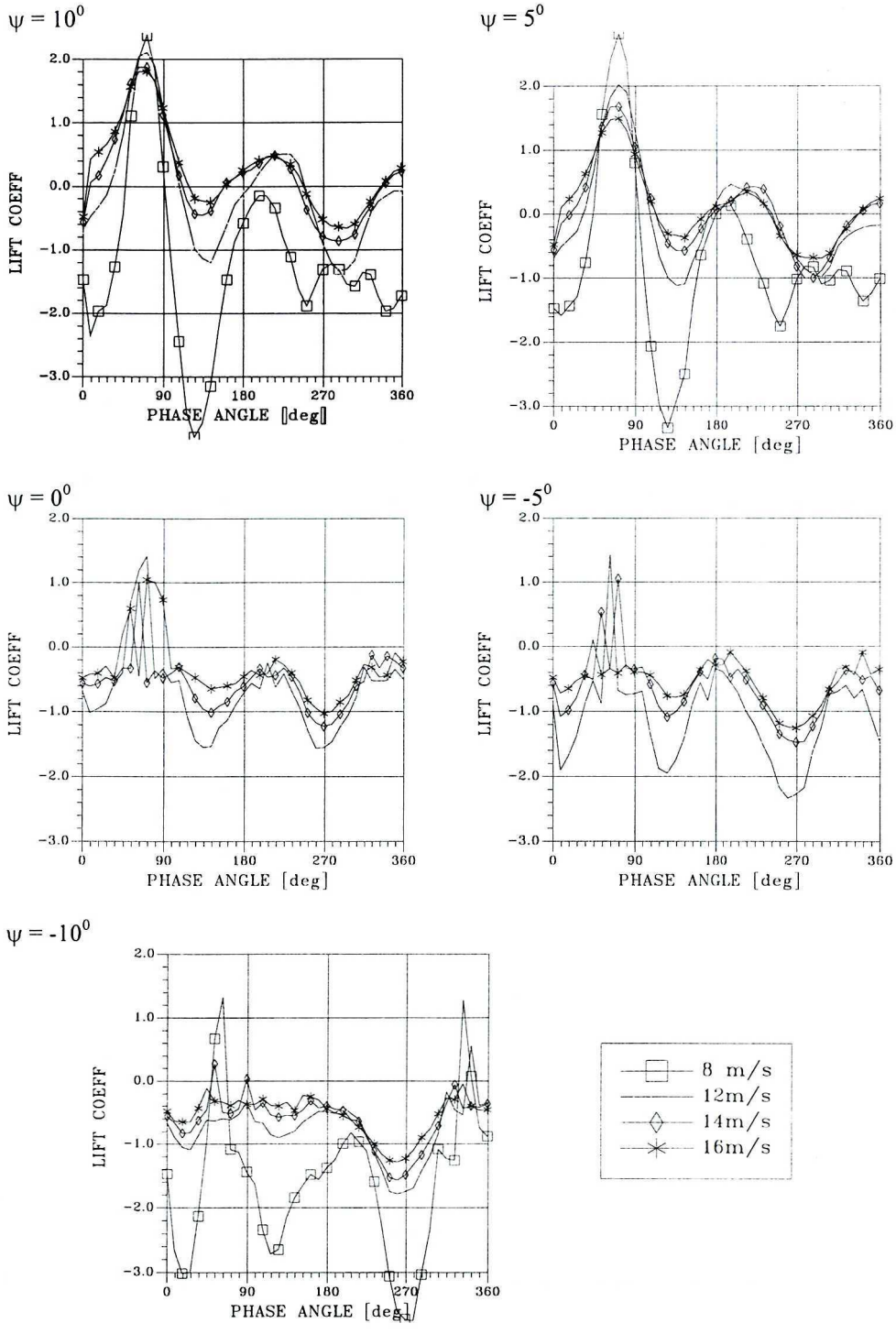

Fig. 13. Unsteady lift coefficients in function of phase angle for: $\Delta\psi = 10^0$, $\psi = 10^0$ to -10^0

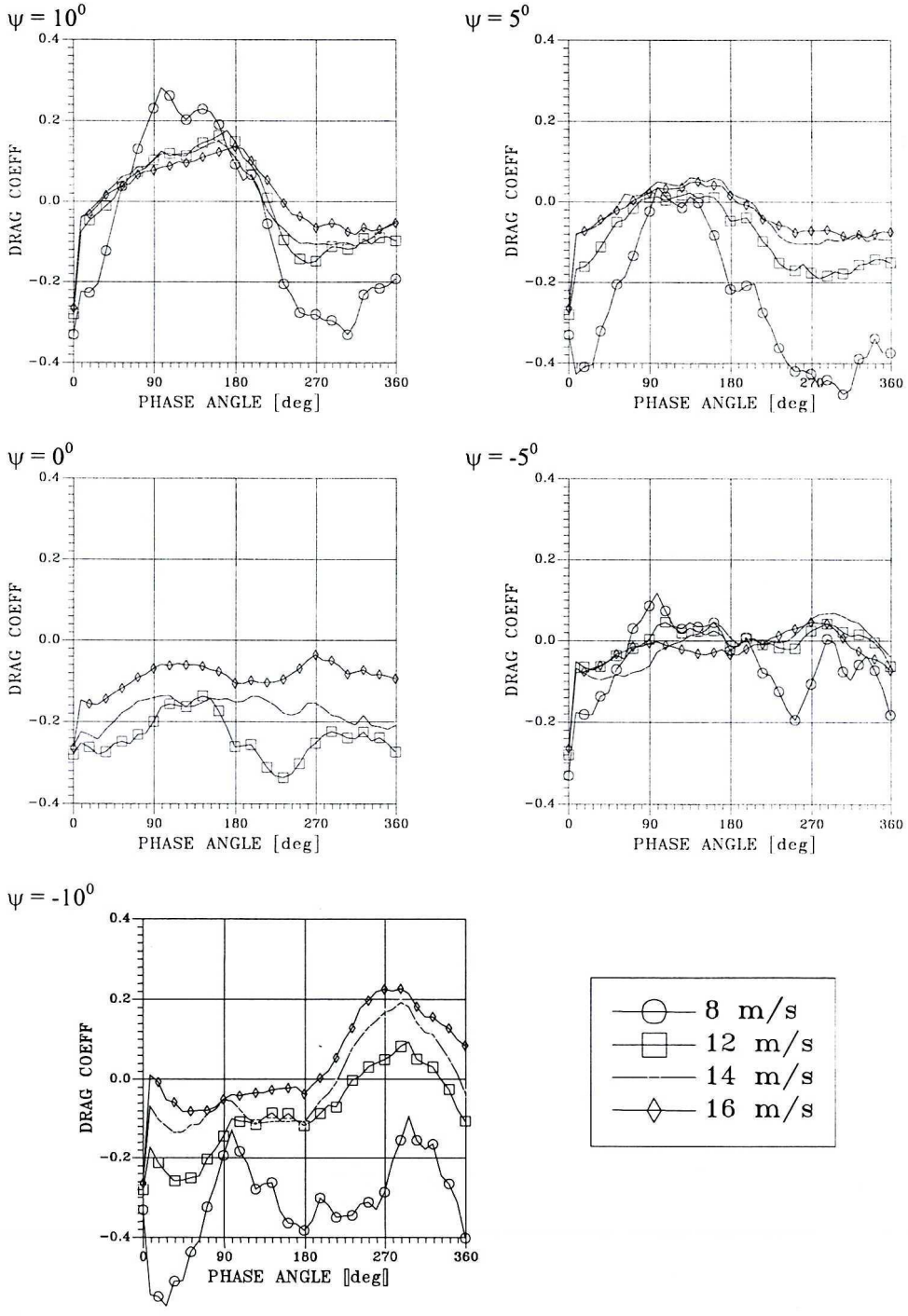

Fig.14. Unsteady drag coefficient in function of phase angle for: $\Delta\psi = 10^0$, $\psi = 10^0$ to -10^0

The formulas used for computation:
LIFT COEF: $Cz = (LIFT - Z0) / qS$
DRAG COEF: $Cx = (DRAG - X0) / qS$
where LIFT & DRAG are taken from Fig. 7 to 10,
qS, Z0, X0 are taken from Tab. 4,
LIFT COEF & DRAG COEF are reported in Fig. 11 to 14.

No computations were done for the case of zero velocity. Nevertheless, the wing movement supplies some air flow around the model, but its velocity and dynamic pressure are not definable.

The negative magnitudes of drag coefficient, visible in the graphs 12 and 14, indicate the generation of thrust in effect of wing movement. The same conclusion refers to the negative drag force visible in the Fig. 8 and 10 for V=0, where the computation of drag coefficient was impossible.

However, the comparison of the corresponding drag graphs shows that the thrust is higher when the flow velocity is lower.

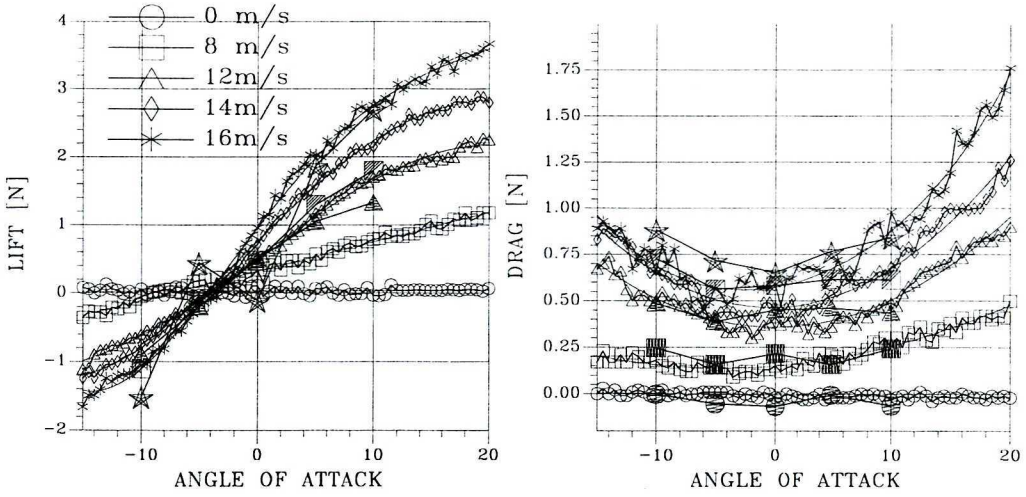

Fig. 15. Lift and drag forces – comparison between static measurements as in Fig. 5 c,d, (continuous lines, small white points) and average values from unsteady measurements (big separate points)

The average magnitudes of dynamic results should in principle be identical with those of static measurements. Nevertheless, their difference (black points in Fig. 15) is too great, resulting, as indicated before, from the poor precision of the measurement of weak forces near to the insensibility zone, and zero drift of the balance system.

The mechanism of the dynamic lift generation can be demonstrated on the example of the specific case of great angle of attack, corresponding to the feathering angle $\psi = 10^0$ and -10^0 and the low velocity V = 8 m/s in Fig. 16 (angle of attack shown in 1/10 scale).

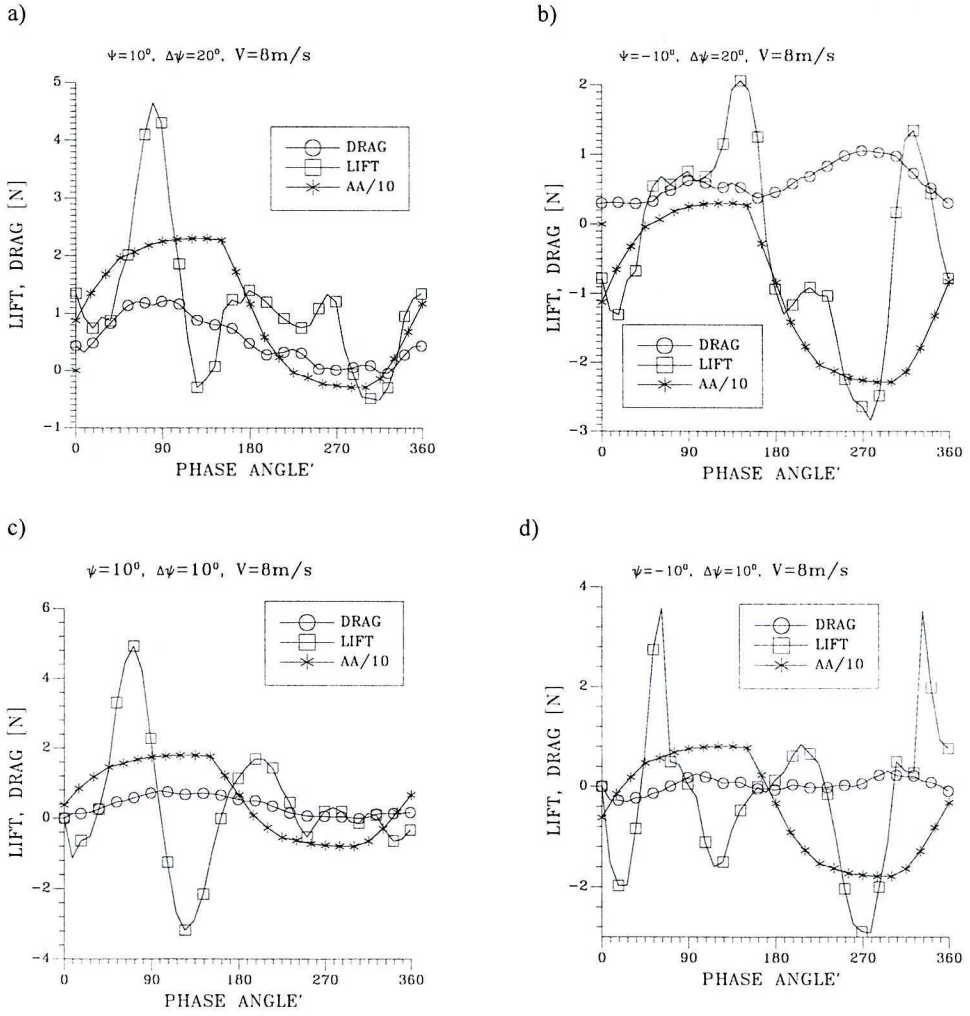

Fig.16. Comparisons between measured lift (○), drag (□), both in Newtons, and angle of attack (*, AA, magnitude in degrees on vertical scale multiplied by 10) for:

a) $\psi = 10^0$, $\Delta\psi = 20^0$, V=8m/s;
b) $\psi = -10^0$, $\Delta\psi = 20^0$, V=8m/s;
c) $\psi = 10^0$, $\Delta\psi = 10^0$, V=8m/s;
d) $\psi = -10^0$, $\Delta\psi = 10^0$, V=8m/s;

The strong maximum (or minimum) of lift coefficient is observed in this figure at the time moment corresponding, roughly, to 30–40^0. This is compatible with the characteristic time t_c in which the fluid element flows (V = 8m/s) along the chord of the profile (c = 0.08m). It can be considered as the time (in order of magnitude) necessary to establish the stationary flow around the wing:

$$t_e = c/V = 0.08 / 8 \approx 0.01 \text{ s} \approx 1/20 \text{ of flapping period} = 18^0.$$

For great values of feathering angle $\psi = 10^0$, when the feathering amplitude is high: $\Delta\psi = 20^0$:

- when α increases, Z force increases (cf. Fig. 7), particularly when $\partial\alpha/\partial\psi$ reaches maximum; in a short time equal $2t_c$ the lift coefficient Cz (cf. Fig. 11) increases up to 2, compatible with a characteristic time for airflow,
- when α stabilizes at the magnitude over 15^0 (at phase angle β over 90^0), Z drops abruptly in effect of flow separation,
- when α falls anew to subcritical value (at $\beta \approx 180^0$), force Z increases again with some histeresis in effect of reattachment,
- when α passes to the negative values, Z increases to the negative course and Cz for short time reaches nearly –2. (cf. Fig. 11).

For negative values of feathering angle $\psi = -10^0$, the maximum of lift appears at the maximum values of α (at phase angle $\beta \approx 150\text{-}180^0$); but when α reaches -20^0 (at β near 270^0), Cz attaints great negative values.

For lower magnitudes of the amplitude of feathering angle $\Delta\psi=10^0$ and higher flow velocities, similar observations can be made with less evidence.

4. Conclusions

1. The results showing the static distribution of aerodynamic forces on the flapping wing were analyzed, at Strouhal number 0.025 to 0.05. Two cases of the amplitude of wing movement, at four velocities, were studied in the range of weak Reynolds numbers (4.10^4 to 8.10^4).
2. The time distribution of aerodynamic forces in function of phase angle of the movement was measured. The corresponding aerodynamic coefficients were estimated.
3. The supposed mechanism of force generation was analyzed.
4. The experimental results, presented here, are not contradictory to those presented by I. Fejtek in [4].
5. The goal of the experiments was to furnish the valuable results for the comparison and validation of the computation by panel method. This computation is being realized by an other team; the first results are not contradictory.

Manuscript received by Editorial Board, May 28, 2002;
final version, September 4, 2002.

REFERENCES

[1] Dial K.P.: An inside look at how birds fly; experimental studies of the internal and external processes controlling flight. 1994 Report to the Aerospace Profession. 38th Symp. Proc., The Beverly Hilton, Beverly Hills, CA, 1994.

[2] Wei Shyy, Mats Berg, Ljunqvist Daniel: Flapping and flexible wings for biological and micro air vehicles. Progress in Aerospace Sciences 35, 1999, pp.455÷505.

[3] Tennekes, H.: The simple science of flight (from insect to jumbo jets). Boston, MA, MIT Press, 1996.

[4] Fejtek I., Nehera J.: Experimental Study of Flapping Wing Lift and Propulsion, Paper No. 709, Aeronaut. Journ., Jan. 1980, pp.28÷33.

[5] Mueller T. J. (ed.): Fixed and Flapping Wing Aerodynamics for Micro Air Vehicle Applications. Progress in Astro.&Aero.Sci., vol. 195, 2001, AIAA Inc.

Badania eksperymentalne sił aerodynamicznych generowanych na modelu ornitoptera

Streszczenie

Wykonano badania eksperymentalne w tunelu aerodynamicznym, obejmujące pomiary siły nośnej i siły oporu na modelu ornitoptera z ruchomymi skrzydłami. Skrzydła wykonywały ruch o dwu stopniach swobody: machanie (wokół osi podłużnej modelu) i przekręcanie (wokół osi podłużnej płatów). Mierzono siły w układzie statycznym – uśredniając pomiar w czasie kilkudziesięciu cykli ruchu, jak również w układzie dynamicznym, mierząc siły nieustalone na płatach w funkcji fazy ruchu. Obliczono odpowiednie wartości współczynników siły i oporu aerodynamicznego.